

参赛队员姓名：袁安琪

中学：北京市十一学校

省份：北京

国家/地区：中国

指导教师姓名：仲国虎/周宏岩

指导教师单位：北京市十一学校

中国科学技术大学

论文题目：Discovery of a galactic fountain
driven by the greatest population of massive
stars

数目最多的大质量恒星驱动的星系喷泉

Abstract

What are stars? Where do they come from? Researches have been investigating on the process of star-formation, and there are still mysteries waiting to explore. The most massive stars, though extremely rare, play a crucial role in helping us determine the mechanism and properties of star-formation. In this study, we focus on the most massive stars, Wolf-Rayet stars, which is the last stage of evolution of O stars before dying. We mainly investigate the galaxy SDSS J1500+4528, and NGC4395 is also studied in order to make comparison with the former. Through analyzing their spectra extracted from the SDSS database, we carefully measure the emission features of both Wolf-Rayet stars and O stars. The numbers of Wolf-Rayet stars in SDSS J1500+4528 is estimated to be $\sim 3 \times 10^6$, which outnumbers previous studies by one order of magnitude. This is very useful to constrain the initial mass function (the relative numbers of newly formed star at various masses). We also discover a galactic fountain in SDSS J1500+4528, where gases are blown out from the galactic plane and then in part pulled back by gravity. This phenomenon, which is found to be associated with a high luminosity Wolf-Rayet galaxy for the first time, reveals itself in the spectrum as an additional blueshift component next to the hydrogen and metal emission lines at rest wavelengths. We argue that the three million Wolf-Rayet stars directly observed in SDSS J1500+4528 are just part of them in an intense starburst, while millions of more massive ones have already died as supernova. Such vigorous supernova explosions naturally drive the “galactic fountain”, typically extending across hundreds of thousands of lightyears.

Contents

| | |
|---|----|
| 1. Introduction..... | 1 |
| 1.1. Massive stars | 1 |
| 1.2. Finding massive stars | 3 |
| 1.3. Aim of this work..... | 5 |
| 1.4. Targets for this study | 5 |
| 1.4.1. Selection of targets..... | 5 |
| 1.4.2. Basic information: SDSS J1500+4528 | 6 |
| 1.4.3. Basic information: NGC 4395 | 7 |
| 2. Data analysis | 8 |
| 2.1. Optical spectra and spectral corrections | 8 |
| 2.1.1. Extinction correction..... | 9 |
| 2.1.2. Correction for redshift | 11 |
| 2.2. Measurement of emission lines | 12 |
| 2.2.1. SDSS J1500+4528 | 12 |
| 2.2.2. NGC4395 | 15 |
| 2.3. Calculation of line luminosities..... | 17 |
| 2.3.1. Calculating line luminosities | 17 |
| 2.3.2. Calculating intrinsic line luminosities | 17 |
| 2.3.3. Estimating the metal abundance of the ionized gas region..... | 19 |
| 2.3.4. Estimating the electron density of the line-emitting gas..... | 19 |
| 3. The number of massive stars..... | 19 |
| 3.1. Estimation of the number of W-R stars | 19 |
| 3.2. Estimation of the number of O stars..... | 20 |
| 3.3. Number of massive stars | 20 |
| 3.3.1. Number of massive stars in SDSS J1500+4528 | 20 |
| 3.3.2. Number of massive stars in NGC4395 | 21 |
| 4. Results and physical interpretation | 22 |
| 4.1. Summary of results..... | 22 |
| 4.1.1. SDSS J1500+4528 | 22 |
| 4.1.2. NGC4395 | 23 |
| 4.2. The greatest population of massive stars and extreme starburst | 23 |
| 4.3. Galactic fountain in SDSS J1500+4528 | 23 |
| 4.3.1. The galactic outflow and fountain | 23 |
| 4.3.2. The driving energy of the outflow | 25 |
| 4.4. Initial mass function of the star-formation | 27 |
| 4.5. NGC4395: a local galaxy with star-forming regions | 28 |
| 5. Summary | 30 |
| References..... | 32 |
| Acknowledgement/致谢..... | 33 |

Figures

| | |
|---|----|
| Figure 1-1 The H-R diagram for stars (figure from internet)..... | 2 |
| Figure 1-2 The basic information for the SDSS observation of the galaxy J1500+4528 (https://dr16.sdss.org/home). | 7 |
| Figure 1-3 The composite optical image of the galaxy J1500+4528 taken in the SDSS survey (from the SDSS webpage). | 7 |
| Figure 1-4 Optical image of NGC 4395 (credit: NOAO, from internet), showing some star-forming regions across the galaxy. | 8 |
| Figure 2-1 The original spectrum of SDSS J1500+4528 (SDSS database website) | 8 |
| Figure 2-2 The original spectrum of NGC4395 (SDSS database website) | 9 |
| Figure 2-3 The schematic description of the radiative transfer (figure from internet)..... | 10 |
| Figure 2-4 The spectrum of SDSS J1500+4528 after correction of the red shift and Galactic extinction (blue). The orange line represents the flux errors: | 11 |
| Figure 2-5 The spectrum of NGC4395 after correction of the red shift and Galactic extinction (blue). The orange line represents the flux errors..... | 12 |
| Figure 2-6 The fitting of the blue bump. The yellow line shows the original spectrum in this region and the blue line shows the resultant shape of the fitting. The three gaussian models at the bottom shows the three emission lines independently..... | 13 |
| Figure 2-7 The fitting of the H_{β} and OIII lines. | 13 |
| Figure 2-8 The fitting of H_{β} using two gaussian models. The green and red shape shows the components of the line. The red gaussian model is the H_{β} line, and the green one is its blue shift component. | 14 |
| Figure 2-9 Fitting the NII doublet and the H_{α} line with one gaussian model each. The blue wing at the bottom of each line is not well fitted. The components are not shown here. | 14 |
| Figure 2-10 The fitting of the NII doublet and the H_{α} using one more gaussian model. The green and purple components represent the NII doublet, and the red one is the H_{α} line. The brown gaussian model shows the blue shift of the H_{α} line. | 15 |
| Figure 2-11 Fitting of the blue bump of NGC4395. The yellow line shows the original spectrum in this region and the blue line shows the resultant shape of the fitting. The red and purple line show the CIV and HeII component independently. The flat green line represents NIII component, which doesn't exist. | 16 |
| Figure 2-12 Fitting of the red bump of NGC4395..... | 16 |
| Figure 4-1 Example of outflowing gas in the famous nearby starburst galaxy M82 (optical light in white-blue color and the hydrogen emission line H_{α} in red). Two large-scale bi-polar outflows (red colored), which are traced by the hydrogen emission lines, are seen perpendicular to the galactic disk. Note that both the bi-polar outflows are seen because the galaxy is viewed from the side of its disk. . | 24 |
| Figure 4-2 Computer simulation of bi-polar galactic fountains formed in a star-forming galaxy. An outflow is launched driven by supernova explosion. The outer part with low speeds turns downwards and fall back. (Figure from internet) | 25 |
| Figure 4-3 The optical image of the star-forming region in the galaxy NGC 4395 that | |

was observed in the SDSS survey. The circle represents the region covered by the observing fiber, with a diameter of 215 lightyears. The light within this area was collected to produce the observed optical spectrum (image provided from the SDSS).29

2020 S.-T. Yau High School Science Award

1. Introduction

1.1. Massive stars

“Twinkle, twinkle, little star, How I wonder what you are!” What are stars? Why are they shining? Where does the energy come from? To answer these questions, we can start from measuring the light of stars. The term of “luminosity” is used to describe the total radiation power of an object. The intrinsic luminosity of a light source is obtained from the measurable brightness (flux f) and distance (D), $L = 4\pi fD^2$. Measurements show that the stars are hundreds to thousands lightyears, or even further, away from us, and many of them are much brighter than our sun. Thus, they must have extremely high energy, and the only energy source possible to support it is nuclear fusion, mostly by combining hydrogen atoms into helium atoms. Stars that burn hydrogen are called main sequence stars.

Stars we see have different colors – some are red and some are blue. It has been known that colors indicate the temperature of radiating bodies. For example, red stars have lower temperature than blue stars. This is because stars radiate as blackbodies, so the wavelength at the radiation peak is determined by temperature. This relationship is shown in Wien’s Displacement Law, as shown in formula (1-1).

$$h\nu_{peak} = 2.8kT \quad (1-1)$$

From "Stefan–Boltzmann" equation, we know the luminosity of a star is related to the surface temperature T and radius R as

$$L = 4\pi R^2 \sigma_{S-B} T^4 \quad (1-2)$$

Also, observations and theories tell us that mass and luminosity are closely linked, as the following relationship,

$$L \sim M^\alpha \quad (1-3)$$

where $\alpha \sim 3$.

Thus, the more massive the stars, the more luminous and the higher temperature. This means that a star can be uniquely represented by one of the three parameters (Maoz 2007).

Main sequence stars are then classified, including O, B, A, F, G, K, M stars based on their temperatures, where O stars have the highest temperature and M stars have the lowest. Table 1-1 shows the parameters of different classes of main sequence stars.

Table 1-1 Types of stars and their parameters

| Class | Surface temperature (K) | color | Mass (solar) | Radius (solar) | Luminosity (solar) | Fraction (%) |
|-------|-------------------------|---------------|--------------|----------------|--------------------|--------------|
| O | ≥ 33,000 | Blue | 16-150 | >6.6 | >30,000 | ~0.0003 |
| B | 10000-33000 | Blue/white | 2.1-16 | 1.8-6.6 | 25-30,000 | ~0.1 |
| A | 7,500-10,000 | White/blue | 1.4-2.1 | 1.4-1.8 | 5-25 | ~0.6 |
| F | 6,000-7,500 | White | 1.0-1.4 | 1.15-1.4 | 1.5-5 | ~3 |
| G | 5,200-6,000 | Yellow | 0.8-1.0 | 0.96-1.15 | 0.6-1.5 | 7.5 |
| K | 3,700-5,200 | Yellow/orange | 0.45-0.8 | 0.7-0.96 | 0.08-0.6 | ~12 |
| M | < 3,700 | Orange/red | <0.45 | <0.7 | <0.08 | ~76 |

The distribution of various types of stars on temperature and luminosity is shown in the so-called Hertzsprung and Russell (H-R) diagram, as shown in the figure below. The band at the middle is the main sequence. Stars spend most of the time throughout their lives on the main sequence since their birth. They only leave when the hydrogen is used up and turn into giants and other types of stars. This process describes star evolution. The stars' lifetime spent on the main sequence (which equals the time of their hydrogen burning phase) depends on the mass of the stars – the more massive the stars, the shorter the lifetimes.

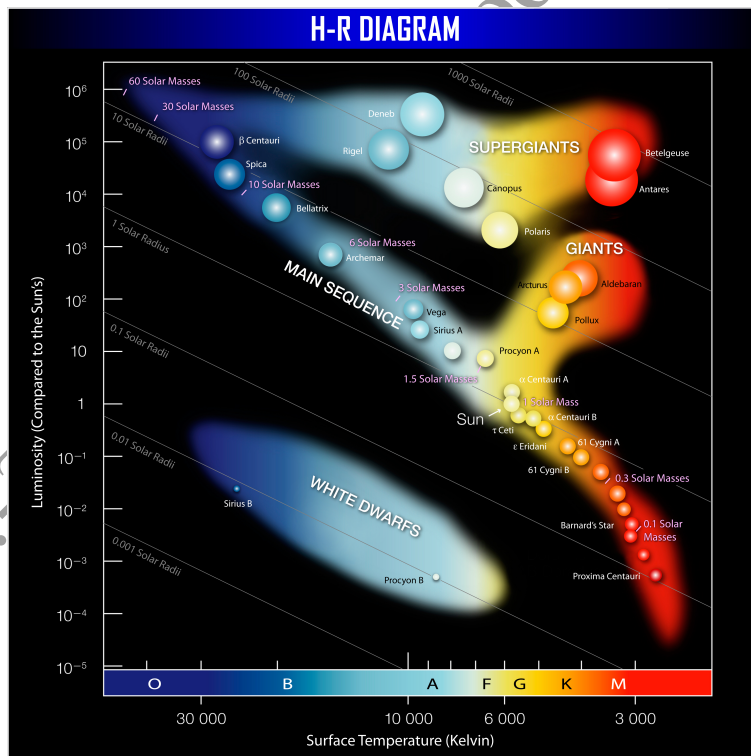


Figure 1-1 The H-R diagram for stars (figure from internet)

The upper left corner of the H-R diagram represents the most massive, the hottest, and the most luminous stars of the entire stellar population, which belongs to the O star type. The most massive of the O stars have the shortest lifetime, about 3×10^6 years, in contrast to $\sim 10^{10}$ years

of the Sun.

Radiation produces pressure on gas due to the scattering and absorption of photons by electrons and atoms/ions. Since O stars have an extremely high radiation, the radiation pressure blows away hydrogen at the outer layer, and leaves the bare helium core at the center, which can be seen directly. Massive O stars at this special stage of late evolution phase are called the Wolf-Rayet (W-R) stars, named after the discoverers Charles Wolf and George Rayet in the 19th century. Only O stars have masses ~ 35 solar mass and above can evolve into W-R stars, and the limit for those who have higher metal abundance (\sim solar abundance) is 25 solar mass. O stars evolve to the W-R phase about 2 to 5 Myr after their birth. The stage of W-R stars last less than 5×10^5 yr, after which they explode and turn their cores into neutron stars or black holes. W-R stars are found to have strong outflows at a high speed, with a mass loss rate of 10^{-4} - 10^{-5} solar mass per year. W-R stars have distinct observational features which will be discussed later.

Massive stars like O stars and W-R stars are extremely rare compared to stars with smaller masses, only about $\sim 0.0003\%$ (Maoz, 2007). Studies show stars in our Galaxy follow a mass distribution described by a powerlaw, which is called the Initial Mass Function (IMF), as shown in(1-4) . For stars in our Galaxy, α equals 2.35 according to Salpeter (1955).

$$\frac{dN}{dm} \propto m^{-\alpha} \quad (1-4)$$

What determines the amount of stars of different masses? This question is not fully understood, but people believe that it is related to the process of how stars are formed.

It is believed that stars are born in giant molecular clouds under some conditions. A huge molecular cloud fragments into numerous dense clumps, then the clumps contract due to their gravitational force, liberating gravitational energy and converting into thermal energy, therefore heats up the gas. The thermal gas produces radiation and resists the gravity pull. If the clumpy cloud is sufficiently large, i.e, the mass larger than the so-called Jeans mass (Maoz 2007), gravity overcomes radiation pressure and collapse proceeds until the hydrogen fusion is triggered in the core where the temperature increases to $\sim 10^7$ K. The fusion reactions release tremendous energy and produce an outward pressure sufficient to halt the inward gravitational contraction, A main sequence star is born.

Although the exact process is not clear, people tend to believe the number of stars formed at certain masses is determined by the fragmentation process of molecular clouds. For smaller fragments, it is easier to reach the Jeans mass criteria and form stars with smaller masses. However, for the larger fragments, further fragmentation may happen if the Jeans criteria cannot be met. As a result, number of massive stars are less than that of smaller stars.

As can be seen, the number of massive stars, including W-R stars and O stars, can constrain the initial mass function, which can further be used to examine theories of star formation (Schaerer & Vacca 1998).

1.2. Finding massive stars

W-R stars can be spotted easily from other stars since they have unique features shown in their optical spectra. W-R stars have broad emission lines in the short wavelength band (mainly 4400-4700Å) and the long wavelength band (mainly 5600-5800Å). This feature is different from

other types of stars, which only have absorption lines in their spectra (some are very weak). The emission lines of W-R stars originate from the hot outflowing matters. The outflows have a high speed, causing the broadening of their lines, due to the Doppler effect. Observations show the outflow speeds can be as fast as ~ 2000 km/s. The two main types of W-R stars are WN and WC stars. WN stars show strong emission lines of helium (He), carbon (C) and nitrogen (N); WC stars show strong He, C, and O emission lines. The WN stars' optical spectra show emission lines from NIII (4640Å), CIV (4650Å), HeII (4861Å), and others. Optical spectra of WC stars show mainly CII, CIII (5696Å), CIV (5808Å), OV (5592Å), HeI, and HeII lines. No nitrogen lines are seen in the WC stars.

Although O stars have weak absorption lines in their spectra, they have strong ultraviolet radiation, arising from their high temperatures. The strong UV radiation of both W-R and O stars can photo-ionize the gas around them, which is leftover debris from star birth. The electrons then recombine with ions and emit photons, which are detected as emission lines, such as H α , H β and OIII. The region where the photoionization and recombination balances is called the HII region. Thus, O stars can be traced in observations by these emission lines, if there is sufficient amount of gas around the stars.

W-R stars are difficult to find, due to their short life and extreme rareness. So far, only ~ 500 individual W-R stars are found in our Galaxy, and a few hundred in neighboring galaxies. At large distances, the angular sizes of galaxies become very small, and stars cannot be resolved individually. W-R stars can only be found collectively as a population from integrated spectra of galaxies or star forming regions, which are contributed by a large number of stars. Galaxies showing W-R features in their spectra are called Wolf-Rayet galaxies (Allen et al. 1976). In observations, W-R galaxies are discovered by finding the W-R emission features in the spectra, which show themselves as two emission bumps in low resolution spectra. The blue bump include a range of emission lines, typically including the NIII 4640, C III/C IV 4650, and He II 4686Å broad W-R lines. The red bump is the broad emission line of CIV at wavelength 5808Å, contributed by WC stars (e.g. Osterbrock & Cohen 1982; Vacca & Conti 1992; Guseva et al. 2000, Zhang 2007). The number of W-R stars present in galaxies can be estimated from the strength of the emission bumps. If a large number of W-R stars are found in a galaxy, it indicates a recent burst of massive star formation in the galaxies.

The first galaxy with the integrated emission feature of Wolf-Rayet stars was identified in 1976 (Allen et al. 1976). Since then, there have been much efforts to search for Wolf-Rayet galaxies (e.g. Osterbrock & Cohen 1982, Conti 1991, Vacca & Conti 1992). Among them, noticeably, the first W-R galaxy catalog including 37 W-R galaxies was compiled by Conti (1991), followed by one including 39 W-R galaxies (Guseva et al. 2000). A more comprehensive catalog containing 139 W-R galaxies was compiled by Schaerer & Vacca (1999) from the literature. With the availability of enormous spectral data for large galaxy samples provided by the SDSS, many more W-R galaxies were found from the SDSS and their number increased significantly since 2000. One important W-R galaxy catalog built from the SDSS DR3 data is the one published by Zhang et al. (2007), which contains 174 W-R galaxies. After that, Brinchmann et al. (2008) claimed to find 570 W-R galaxies from SDSS DR6 at low redshifts (relatively nearby distances). A search of W-R galaxies from a sub-class of galaxies called blue compact galaxies from the SDSS DR7 data was reported by Agienko et al. (2013), however, without publishing their source catalog. Although the later studies using the SDSS DR6-7 data claimed to find several hundreds

W-R galaxies, some of them are only candidates with uncertainties in their identifications (see their papers). Most recently, Liang et al. (2020) published a catalog containing 90 W-R galaxies with 276 starforming regions at redshifts $z < 0.15$, using the IFU (integrated field unit) data obtained in the MaNGA program of the SDSS; however, no numbers of W-R stars were given, nor quantities usable for their estimation.

As results out of these W-R galaxies, the number of W-R stars found in a galaxy ranges from several tens to the order of 10^5 . One of the reasons why there were no much more W-R stars than the maximum numbers found in previous work is perhaps due to that: the previous searches were in galaxies in the local universe, within redshift $z < 0.2$. Since galaxies with much more W-R stars must be very rare, one must search for more galaxies within a much larger distance range. That is to say, a large database must be searched to larger distances than those in previous work.

1.3. Aim of this work

In observations, massive stars are extremely rare (due to their small amount of formation, fast evolution, and short lives), giving rise to a large uncertainty at the most massive part of the IMF of stellar population. This is one of the difficulties we face when studying star-formation. Searching for massive stars can improve the understanding of the initial mass function, providing new observational evidence to test the theory of star formation.

Common studies on massive stars focus on ongoing and recent star-forming galaxies. The massive stars newly formed in these galaxies are inferred *indirectly* from the other features rather than the stars themselves. These include typically optical hydrogen emission lines from gas ionized by massive stars or the thermal emission in the infrared from warm dust heated by them. The disadvantage of this approach is that the massive stars cannot be measured directly. Moreover, an active nucleus powered by a supermassive black hole can contribute to emissions we observed, causing confusion in studies in some cases.

In contrast, with the directly observable features, W-R stars could trace massive stars in ongoing or recent star-formation. It can also mark the stellar population's age. If there are more W-R stars, star forming rate in the galaxy is higher. A large amount of W-R stars can unambiguously indicate strong star formation. However, previous studies in this approach only found small to moderate numbers of W-R stars, associated with weak or moderate star-forming activities in galaxies.

In this research, we aim at, taking the second approach, studying massive stars in more intensive starforming (or even starburst) sites, by finding a much larger population of W-R stars, than those ever achieved in previous studies.

1.4. Targets for this study

1.4.1. Selection of targets

Our immediate goal is to find galaxies with more W-R stars than what have been known. Since W-R galaxies are very rare and difficult to find, the largest database of optical spectroscopic observations, the Sloan Digital Sky Survey (SDSS, <https://www.sdss.org>), would be ideal for the

search. The SDSS is a large multi-spectral imaging and spectroscopic redshift survey using a dedicated 2.5-m wide-angle optical telescope. The telescope is equipped with spectrographs covering a wide wavelength range in the optical band. The spectrographs connected to the telescope through ~600 optical fibers to transmit the collected light of ~600 targets imaged on the focal plane by the telescope. The SDSS began regular survey operations in 2000. It is now in the SDSS-IV phase (2014-2020). All its data are open to the public and the current data release (DR) is DR16. We search our candidates from the newest data release of SDSS publicly available (DR16; see <https://www.sdss.org/dr16/>).

Since there are a huge number of observed optical spectra, it is impossible to search through the spectra of all the objects. To achieve our goal more efficiently, we used a different approach from what have been used in previous work by the others (e.g. Zhang et al. 2007). Galaxies undergoing intensive star-formation are typically bright in the infrared, emission that arises from warm dust surrounding and heated by the strong radiative energy of young massive stars (O, B and W-R stars) just formed. The more stars, the brighter the galaxies in the infrared. We therefore first select objects in the SDSS database that are the brightest in the infrared band in the source catalog of the WISE satellite (<https://wise2.ipac.caltech.edu/docs/release/allsky/>). Then we examine the spectra of these individual objects manually the characteristics blue and red emission bump features of Wolf-Rayet stars.

This procedure resulted in several objects out of our first preliminary attempt. Among them, one object at a large distance, SDSS J1500+4528, stood out with a possible emission feature at the wavelength of the W-R blue bump. We hence take it as a candidate W-R galaxy for study in this work.

In the course of the searching, a spectrum targeting one of the star-forming regions in a nearby galaxy NGC 4395 was also noticed of showing W-R bump-like features. The spectral quality is high enough to ensure the robustness of the analysis results. Since star-forming regions in (other) nearby galaxies have been studied in great details, their results can be compared to that for NGC 4395, as a check for the reliability of our analysis. It would also be interesting to compare the results for possible massive stars in this nearby galaxy with those in the distant galaxy SDSS J1500+4528. We thus also include this spectral data for NGC 4395 in this work.

1.4.2. *Basic information: SDSS J1500+4528*

We get the information for this object by query from the NASA/IPAC Extragalactic Database (NED, <https://ned.ipac.caltech.edu>). The galaxy SDSS J1500+4528 (full name SDSS J150009.81+452844.4) was observed in the SDSS eboss survey with its images and spectrum taken. Its sky coordinates, and the observation information can be found in the SDSS data webpage as shown in the Figure 1-2. It is a distant galaxy with a redshift 0.4532 caused by the expansion of the universe, as measured by the SDSS data reduction pipeline and corresponding to a distance of 5.711 Giga-lightyears (5.4×10^{25} meters). Its image in visual band taken in the SDSS is shown in Figure 1-3, which is almost unresolved for such a far object.

The screenshot shows the SDSS Science Archive Server (SAS) interface. At the top, there is a navigation bar with links for Home, Imaging, Optical Spectra, Infrared Spectra, and MaStar Spectra. A 'SAS Login' button is in the top right. Below the navigation bar, there are tabs for 'Basic Search', 'Bulk Search', 'Bitmasks', and 'Spectrum Parameters'. The 'Spectrum Parameters' tab is active, displaying a table of object parameters for 'eBOSS Specobj'. The parameters include Survey (eboss), Plate (8490), MJD (57104), FiberID (786), RA (15:00:09.81), DEC (+45:28:44.49), Version (v5_13_0), bestobj_id (1237662500537041031), specobj_id (-8887637691394142208), z (0.453235), zerr (3.50825e-05), Class (QSO), and Subclass (STARBURST). To the right, there are search options for Redshift (z, z_noqso), RA/Dec (Sexagesimal, Decimal), RA / Dec Search Range (arcmin), and Download spec as (lite, full). Below the search options, there are links for 'spec data model' and 'CAS'. At the bottom, there are navigation buttons for 'Previous Spectrum' and 'Next Spectrum', and a file download link 'spec-8490-57104-0786.fits'. The status bar indicates 'Showing 636 of 808 Spectra for this view'.

Figure 1-2 The basic information for the SDSS observation of the galaxy J1500+4528 (<https://dr16.sdss.org/home>).

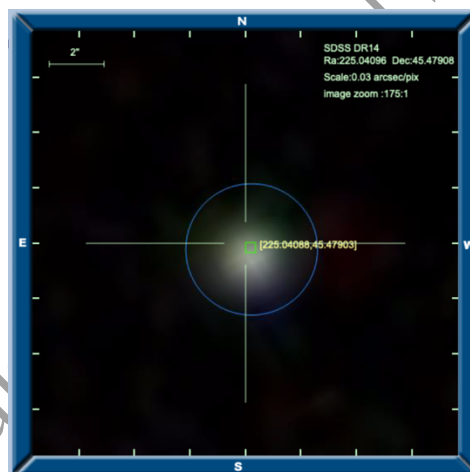


Figure 1-3 The composite optical image of the galaxy J1500+4528 taken in the SDSS survey (from the SDSS webpage).

1.4.3. Basic information: NGC 4395

The following information is extracted from the NED database as above. NGC 4395 is a spiral galaxy in irregular shape, with a size of 6.5×10^4 lightyears in diameter, located at a distance of only 15.04 lightyears (1.42×10^{23} meters) away. Figure 1-4 shows its optical image got from internet. It has low surface brightness, meaning small density of stars on the galaxy disk. There are many bright spots scattered on the galaxy disk, which are concentrations of many stars. Some are the sites where new stars are just formed (star-forming regions).



Figure 1-4 Optical image of NGC 4395 (credit: NOAO, from internet), showing some star-forming regions across the galaxy.

2. Data analysis

2.1. Optical spectra and spectral corrections

The original spectra of the two targets are extracted from the SDSS data archive. In our work, we write Python code to analyze the spectra. First, the spectra need to be corrected for the Galactic extinction and redshift effects. The original spectra of the two galaxies from SDSS are shown below.

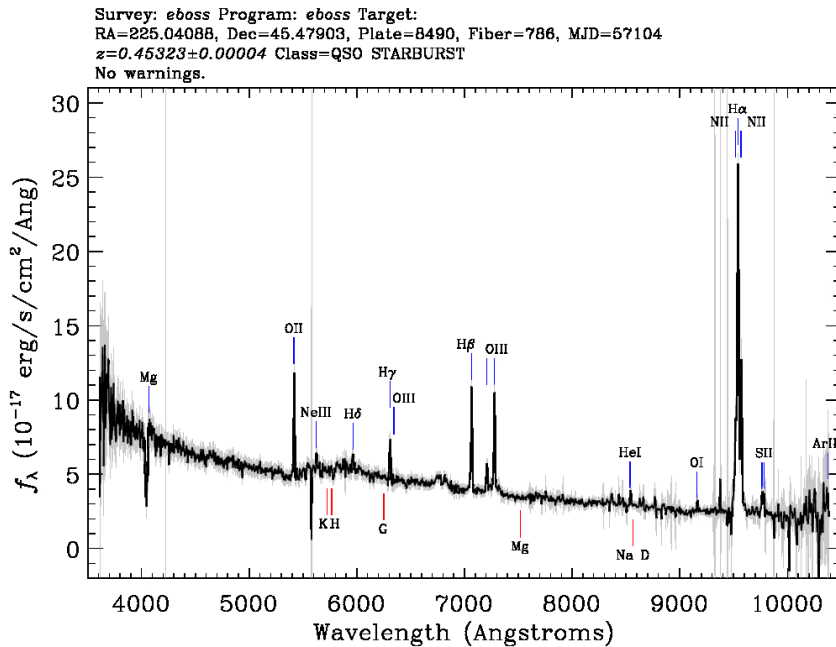


Figure 2-1 The original spectrum of SDSS J1500+4528 (SDSS database website)

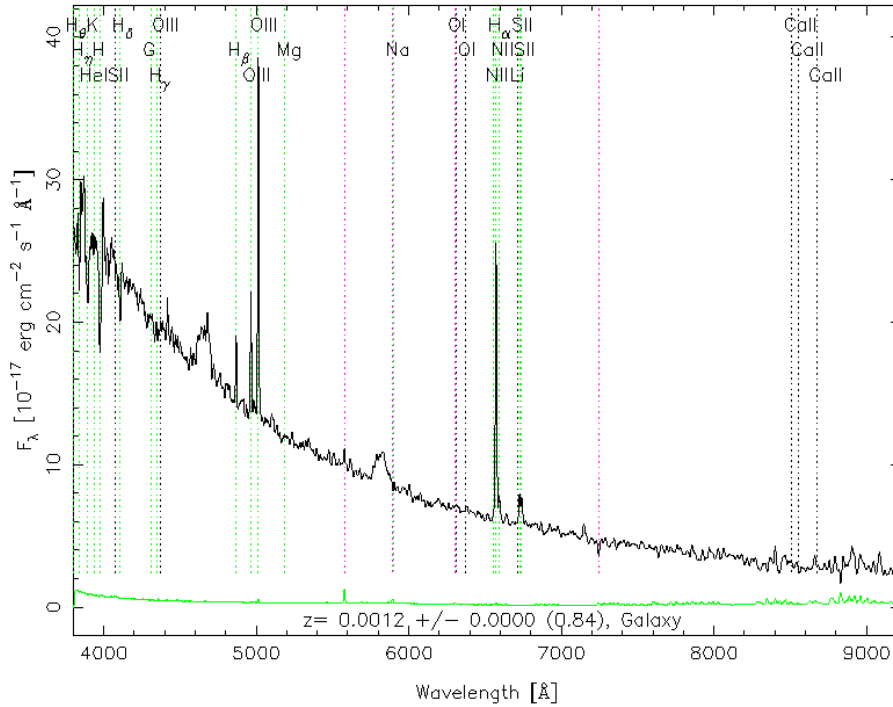


Figure 2-2 The original spectrum of NGC4395 (SDSS database website)

2.1.1. Extinction correction

Extinction is the absorption and scattering of electromagnetic radiation by dust and gas between the observer and the emitting object. Stars behind a lot of dust look redder than they actually are, since blue light is much more strongly attenuated than red light by dust extinction. This is similar to the red sunset owing to the extinction by dust particles in the atmosphere of the Earth. Thus, the interstellar extinction is often called interstellar reddening. For Earth-bound observers, the Earth's atmosphere and the circumstellar dust around the observed object cause extinction.

As a consequence of extinction, the observed flux is reduced and the shape of the observed spectrum is distorted. To obtain the intrinsic luminosity and spectrum of a star, extinction correction is necessary.

As show in Figure 2-3, when light travels in dust, the loss of intensity ($-dI(\lambda)$) caused by extinction is proportional to the distance (ds) it travels, the intensity ($I(\lambda)$), the number density (N) and the cross section ($\sigma(\lambda)$) of dust (Maoz 2007),

$$-dI(\lambda) = N\sigma(\lambda)I(\lambda)ds = I(\lambda)d\tau(\lambda),$$

where $d\tau(\lambda) = N\sigma(\lambda) ds$ is the differential optical depth and $\tau(\lambda) = \int_0^s N\sigma(\lambda) ds$ is the optical depth of the dust with a thickness of s .

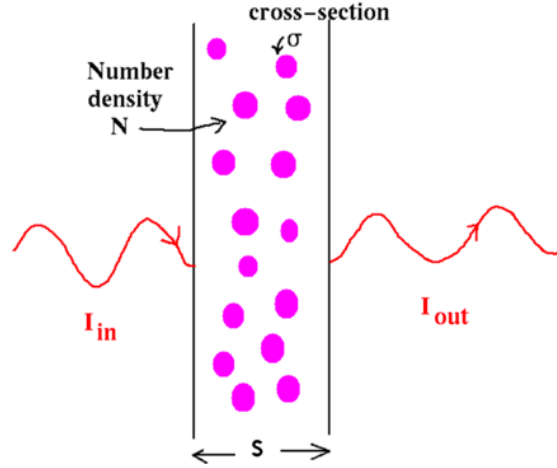


Figure 2-3 The schematic description of the radiative transfer (figure from internet)

Integrating the above equation, we get the radiative intensity after extinction (I_{out}):

$$I_{out}(\lambda) = I_{in}(\lambda)e^{-\tau(\lambda)}$$

For a given extinction curve, $\tau(\lambda)$, the intrinsic intensity of a star can be calculated from the observed intensity, so is the flux $F(\lambda)$ (since $F \propto I$ for distant stars),

$$F_{ob}(\lambda) = F_{in}(\lambda)e^{-\tau(\lambda)}$$

Therefore, the intrinsic flux from an object can be calculated from the observed flux,

$$F_{in}(\lambda) = F_{ob}(\lambda)e^{\tau(\lambda)} \quad (2-1)$$

The procedure above is extinction correction.

For Galactic extinction, it is commonly described using extinction magnitude, $A(\lambda)$, instead of $\tau(\lambda)$. Converting the flux into magnitude in formula $F_{ob}(\lambda) = F_{in}(\lambda)e^{-\tau(\lambda)}$, we get the relationship between $A(\lambda)$ and $\tau(\lambda)$.

$$m_{ob}(\lambda) - m_{in}(\lambda) = -2.5 \log e^{-\tau(\lambda)} = 1.086\tau(\lambda) \equiv A(\lambda)$$

or

$$m_m(\lambda) = m_{ob}(\lambda) - A(\lambda) \quad \text{and} \quad A(\lambda) = 1.086\tau(\lambda)$$

and the intrinsic magnitude of a star is calculated from the measured one and the extinction $A(\lambda)$.

Here we correct for the Galactic extinction, i.e. extinction from the interstellar medium in our Galaxy along the line of sight towards the target. The general shape of extinction curve in the Milky Way from 1250\AA to 35000\AA is well measured and the visual band (V band) extinction can be expressed by the color excess, $E(B - V)$,

$$A(V) = 3.1 E(B - V) .$$

The extinction $A(\lambda)$ at any wavelength in optical/UV can be calculated from a known extinction curve of our Galaxy once the extinction value $A(V)$ or $E(B-V)$ is known for any object. We use the Galactic extinction curve given by Fitzpatrick (1999). We obtained the color excess $E(B - V)$ for our targets from the NED data base: $E(B - V) = 0.0158$ for SDSS J1500+4528, and $E(B - V) = 0.0137$ for NGC 4395. We used the python package *extinction* provided by *astropy* (<https://extinction.readthedocs.io/en/latest/>) to perform the Galactic extinction correction. Note that the extinction due to Earth atmosphere has already been corrected in the SDSS spectra provided. The correction for extinction due to circumstellar dust in the galaxy (internal extinction)

would be described in section 2.3.2.

2.1.2. Correction for redshift

It is known that all the galaxies are moving fast away from us due to the expansion of the universe. The velocity of the galaxy influences the spectra we observe. According to the Law of Doppler effect, if a light emitting object is going away from us, the wavelength of the light is shifted to a longer wavelength, or becomes redder. This effect is called redshift. On the other hand, if it is coming towards us, it has a blue shift (the wavelength becomes shorter). Therefore, the wavelengths of the observed spectra need to be corrected into the original wavelengths (rest wavelengths). The redshift (z) is defined as

$$z \equiv \frac{\lambda_{ob} - \lambda_{rest}}{\lambda_{rest}} = \frac{v}{c}$$

where v is the velocity of the light emitting object (this is the non-relativistic approximation where $v \ll c$). The rest wavelength is then calculated from

$$\lambda_{rest} = \frac{\lambda_{ob}}{1 + z}$$

We perform redshift correction for the two targets using the redshift values available from the SDSS data archive, $z = 0.4532$ for SDSS J1500+4528 and $z = 0.0012$ for NGC4395.

The two spectra after correction for extinction and redshift effects are shown in Figure 2-4 for SDSS J1500+4528 and Figure 2-5 for NGC4395.

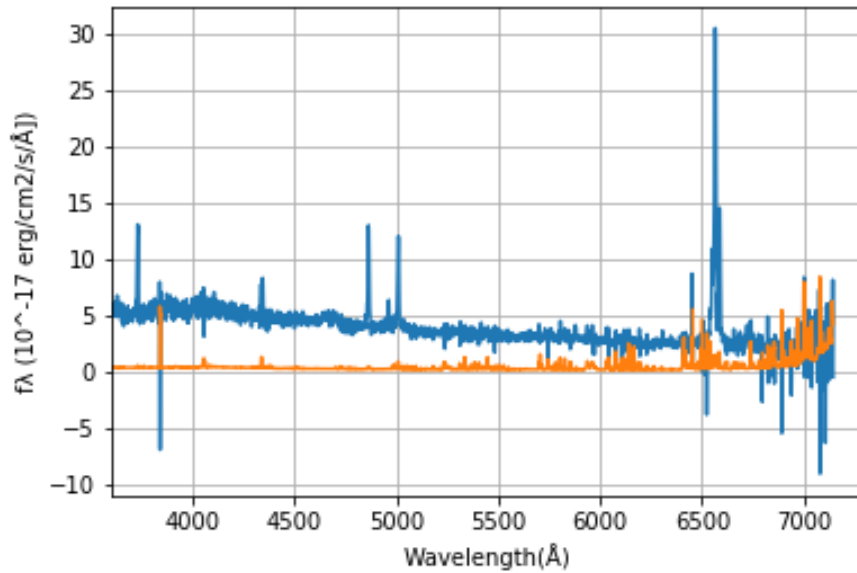


Figure 2-4 The spectrum of SDSS J1500+4528 after correction of the red shift and Galactic extinction (blue). The orange line represents the flux errors.

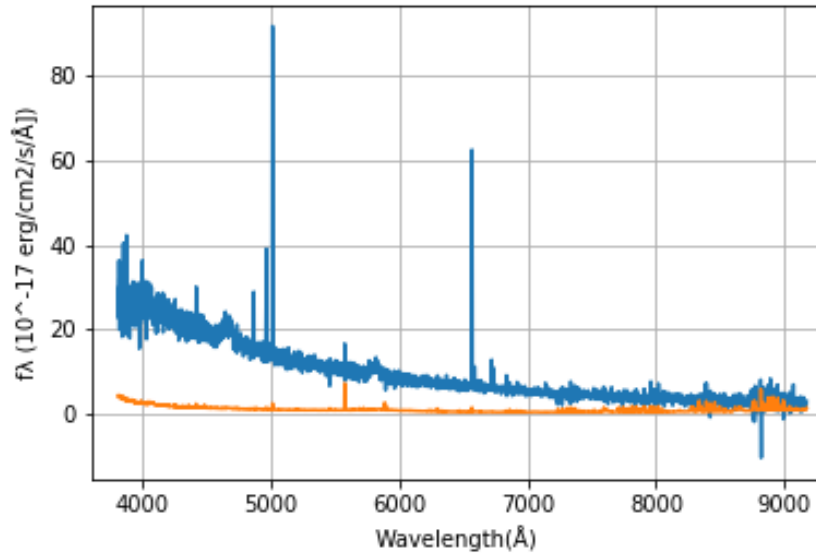


Figure 2-5 The spectrum of NGC4395 after correction of the red shift and Galactic extinction (blue). The orange line represents the flux errors.

2.2. Measurement of emission lines

In the spectra, some strong, narrow emission lines can be clearly seen, including mainly the Balmer recombination lines from hydrogen (the $H\beta$ line at 4861\AA and $H\alpha$ line at 6563\AA), the collisional excited lines of oxygen ions (OIII) at 4959 and 5007\AA , NII (6548 and 6583\AA) and SII (6717 and 6731\AA) in the spectra.

In addition, the blue bump of the W-R feature is clearly visible in both spectra, while the red bump is seen only in that of NGC4395. The blue bump includes emission lines of NIII, CIV, HeII with wavelength 4640\AA , 4650\AA , and 4686\AA . The carbon-type W-R stars, WC stars, contribute to the CIV and He II line, and nitrogen-type WN contribute to all of them. The red bump is the emission line of CIV at wavelength 5808\AA , which comes only from WC stars. Thus, these two galaxies are truly W-R galaxies. In the following, we analyze the emission line properties in detail in order to learn more about the W-R star population and their surrounding gas.

2.2.1. SDSS J1500+4528

We use a power-law model to fit the continuum spectra, and add gaussian models on it to fit the emission lines. The gaussian model contains three variables: area, rest wavelength, and linewidth (represented by the velocity of the Doppler broadening). The integral of the gaussian model equals the flux of the emission line.

For the blue bump, the wavelength of the three emission lines are fixed at 4640 , 4650 , and 4686\AA (NIII, CIII/CIV, and HeII, respectively). The W-R features are obviously detected, as shown in Figure 2-6. The spectrum is well fitted by the model.

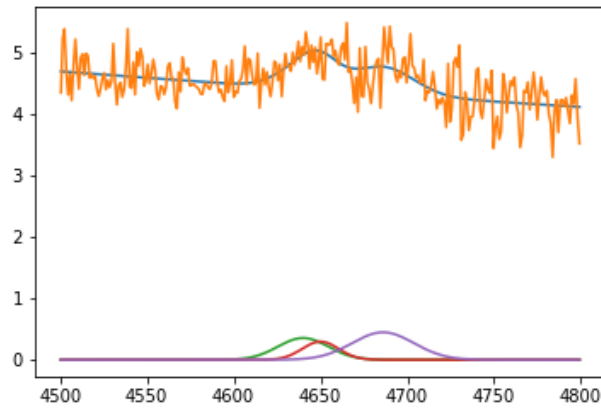


Figure 2-6 The fitting of the blue bump. The yellow line shows the original spectrum in this region, while blue line represents the resultant shape of fitting. The three gaussian models at the bottom shows the three emission lines independently.

For the red bump, the wavelength is fixed at 5808Å. However, the red bump is not detected. We fit the H_{β} , OIII4959 and 5007 lines of ionized gas using a gaussian model each. We find that one gaussian cannot model the spectrum profile very well. The lines are not symmetric, showing excess emission at the blue wing. Also, the peak of the line profile cannot be accounted for. This problem is the same for all the strong lines, including H_{β} , H_{α} , and OIII lines. An example is shown for the H_{β} line and the two OIII lines, as shown in Figure 2-7. The profile of H_{β} line is fitted much better using two gaussian curves, and the blue wing is also well described. The best fit model is shown in Figure 2-8. We can clearly see that the gaussian model of the component sets at both sides of the rest H_{β} line. This means that there are a blueshift and a redshift component. The blueshift of $\Delta\lambda = 3\text{\AA}$, corresponding to velocity 190 km/s. The blue-shifted component is also broad with a linewidth of 900 km/s (fullwidth at half maximum). The same blue-shift component can be found in other strong emission lines, including OIII.

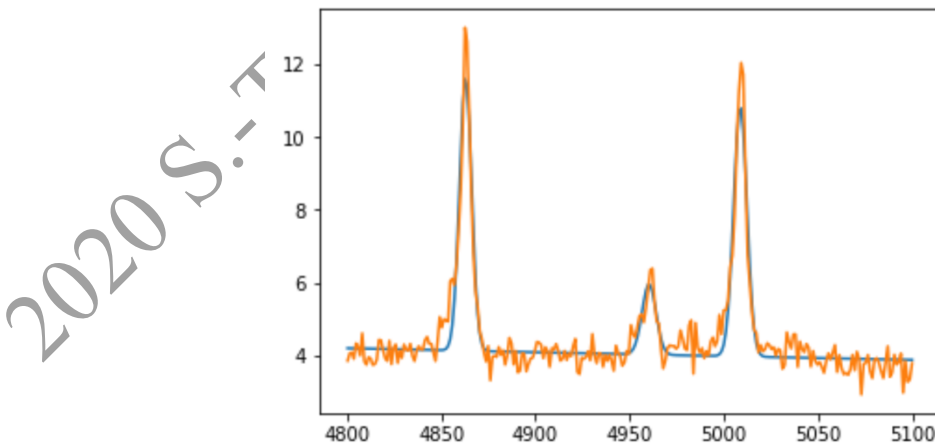


Figure 2-7 The fitting of the H_{β} and OIII lines.

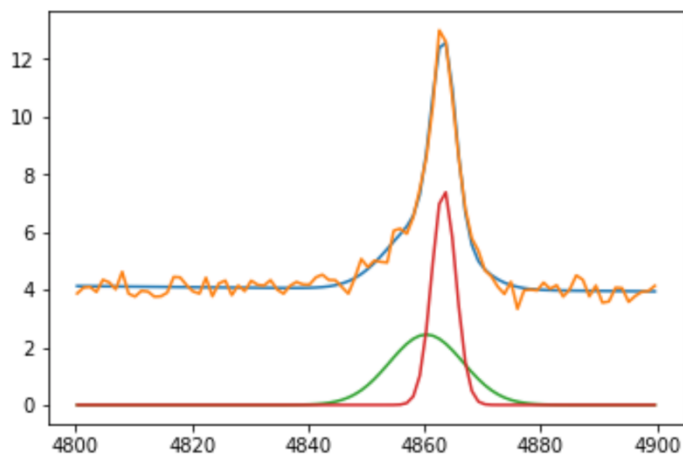


Figure 2-8 The fitting of H_{β} using two gaussian models. The green and red shape shows the components of the line.

The red gaussian model is the H_{β} line, and the green one is its blue shift component.

Fitting the H_{α} line is complicated due to the NII doublet (6583 and 6548Å) being close to H_{α} . The wavelength and the linewidth of the NII doublet are tied. First, we use one gaussian model to fit each line, and the result is shown in Figure 2-9. Then, we add one gaussian model to fit the blue shift of H_{α} line, and the blue shifts of the NII double are ignored because they are too small. The fitting of the blue shift uses the same blue shift velocity and linewidth as that of the H_{β} line. Foigure 2-10 shows the resultant fitting, which is better than the previous one.

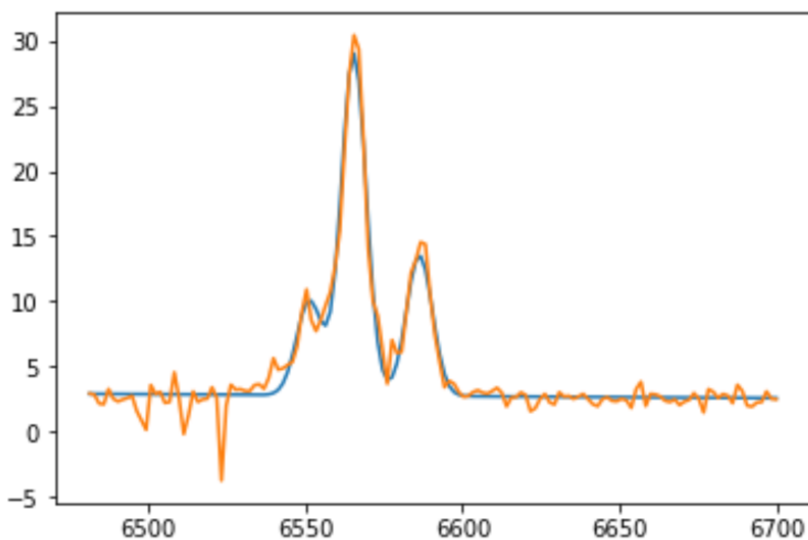


Figure 2-9 Fitting the NII doublet and the H_{α} line with one gaussian model each. The blue wing at the bottom of each line is not well fitted. The components are not shown here.

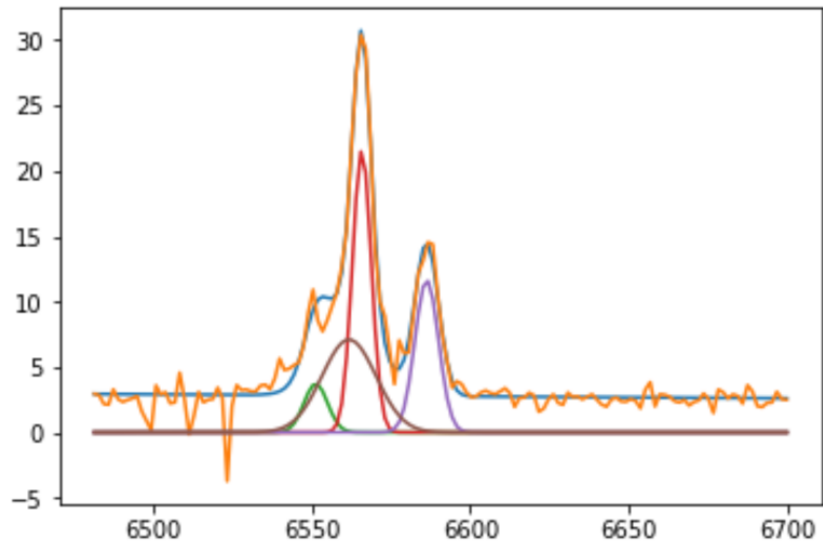


Figure 2-10 The fitting of the NII doublet and the H α line using one more gaussian model. The green and purple components represent the NII doublet, and the red one is the H α line. The brown gaussian model shows the blueshift of the H α line.

Table 2-1 lists the fitted parameters of the emission features.

Table 2-1 Fitted parameters of the emission lines in SDSS J1500+4528

| | Flux ($10^{-17} \text{ erg/cm}^2/\text{s}$) | Fwhm (km/s) | Line Luminosity (10^{40} erg/s) | Intrinsic Luminosity ($\tau_v = 1.76$) (10^{41} erg/s) | Intrinsic Luminosity ($\tau_v = 2.47$) (10^{41} erg/s) |
|-----------------|--|----------------|---|---|---|
| 4640 NII | 12.84 | 2197 | 17.7 | 10.9 | 24.3 |
| 4650 CIV | 7.763 | 1587 | 6.97 | 6.59 | 14.6 |
| 4686 HeII | 19.97 | 2681 | 21.0 | 16.8 | 37.1 |
| H β blue | 38.71 | 919.1 | 45.4 | 31.0 | 67.1 |
| 4861 H β | 33.77 | 299.8 | 39.6 | 27.0 | 58.5 |
| 4959 OIII | 17.89 | 526.1 | 20.9 | 13.9 | 29.9 |
| 5007 OIII | 60.68 | 498.5 | 71.1 | 46.6 | 99.5 |
| 6548 NII | 34.72 | 401.4 | 40.7 | 19.3 | 36.2 |
| H α blue | 152.0 | 919.1 | 178 | 84.5 | 158 |
| 6563 H α | 160.9 | 319.8 | 189 | 89.4 | 167 |
| 6583 NII | 109.3 | 401.4 | 128 | 60.5 | 113 |
| 6717 SII | 14.76 | 351.9 | 17.3 | 8.00 | 14.8 |
| 6731 SII | 14.82 | 351.9 | 17.4 | 8.01 | 14.8 |

2.2.2. NGC4395

We use the same methods to fit the spectrum of NGC4395. The fitting of blue bump shows

only two broad emission lines, the CIII/CIV and HeII line at 4650 and 4686Å. NIII line at 4640Å is not detected. There is a broad red bump in NGC4395 at 5080Å coming from CIV. The fitting of the blue bump and the red bump is shown in Figure 2-11 and Figure 2-12

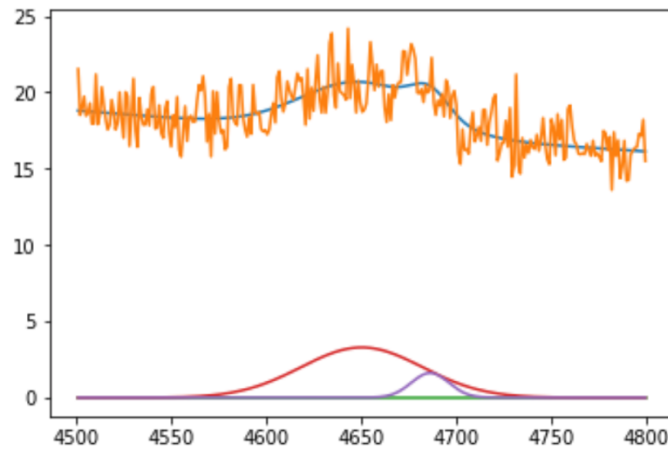


Figure 2-11 Fitting of the blue bump of NGC4395. The yellow line shows the original spectrum, and the blue line represents the resultant shape of the fitting. The red and purple line show the CIV and HeII component independently. The flat green line represents NIII component, which doesn't exist.

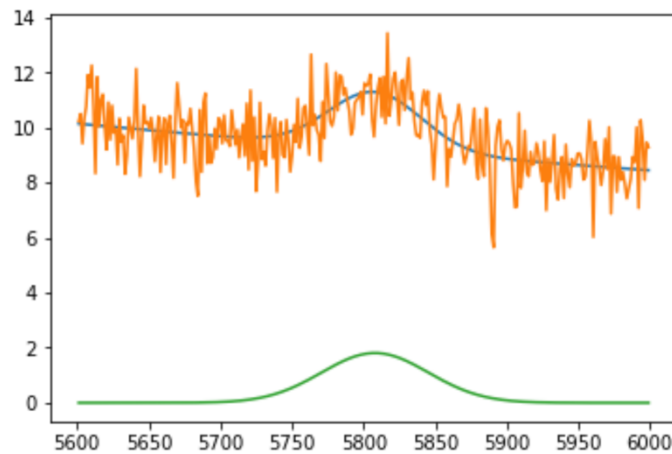


Figure 2-12 Fitting of the red bump of NGC4395.

The other strong emission lines are symmetric and have no blue shift components. Compared to that of SDSS J1500+4528, the OIII line at 4959 and 5007Å and H α line at 6563Å are very strong.

Table 2-2 Fitted parameters of the emission lines in NGC 4395

| | Flux ($10^{-17} \text{ erg/cm}^2/\text{s}$) | Fwhm (km/s) | Line Luminosity (10^{36} erg/s) | Intrinsic Luminosity (10^{36} erg/s) |
|-----------------|--|----------------|--|---|
| 4640 NII | 0 | | 0 | 0 |
| 4650 CIV | 263.8 | 4860 | 6.72 | 132 |
| 4686 HeII | 40.00 | 1490 | 1.02 | 19.6 |
| 4861 H β | 46.85 | 168.2 | 1.19 | 21.3 |
| 4959 OIII | 78.79 | 174.4 | 2.01 | 34.5 |
| 5007 OIII | 245.3 | 174.4 | 6.24 | 105 |
| 5080 CIV | 169.4 | 3939 | 4.31 | 55.0 |
| 6548 NII | 5.043 | 170.2 | 0.128 | 1.33 |
| 6563 H α | 242.8 | 170.2 | 6.18 | 64.0 |
| 6583 NII | 19.46 | 170.2 | 0.495 | 5.10 |
| 6717 SII | 27.00 | 163.4 | 0.687 | 6.86 |
| 6731 SII | 19.45 | 163.4 | 0.495 | 4.92 |

2.3. Calculation of line luminosities

2.3.1. Calculating line luminosities

Luminosity is the total power radiated from a source in all the directions (4π solid angle). Luminosity of an object can be calculated from its flux f and distance d to the Earth.

$$L = f \times 4\pi D^2 \quad (2-2)$$

The calculation of luminosity can be applied for both the integrated continuum emission within a waveband and emission lines. For distant galaxies like SDSS J1500+4528 with relatively large redshifts, the luminosity distance is used, which can be calculated using the redshift z assuming a cosmological model (<http://www.astro.ucla.edu/~wright/CosmoCalc.html>) (using the Hubble constant of 69.6). The luminosity distance of SDSS J1500+4528 is 5.711 Giga-lightyears (5.4×10^{25} meters) for $z=0.4532$. For NGC4395, we adopt a distance of 15.04 lightyears (1.42×10^{23} meters) from the NED database. The luminosities of the emission lines are calculated and recorded in Table 2-1 for SDSS J1500+4528 and Table 2-2 Fitted parameters of the emission lines in NGC 4395. These are the luminosities without correction for the internal extinction caused by dust in the galaxies.

2.3.2. Calculating intrinsic line luminosities

To calculate the intrinsic line luminosity, the extinction caused by circumstellar dust in the galaxy needs to be corrected. The intrinsic flux is given by $F_{in}(\lambda) = F_{ob}(\lambda)e^{\tau(\lambda)}$, so we need to calculate optical depth $\tau(\lambda)$ at any wavelength in the spectral range. In this work, we adopt a

power-law extinction curve which is commonly used for extinction in star formation galaxies (Charlot & Fall 2000).

$$\tau(\lambda) = \tau_V \left(\frac{\lambda}{5500} \right)^\alpha, \quad \alpha = -0.7 \quad (2-3)$$

τ_V is determined by comparing the observed ratio of hydrogen H α line and H β line, $\frac{F_{ob}(H\alpha)}{F_{ob}(H\beta)}$ (this ratio is called Balmer decrement) with the theoretical (intrinsic) ratio of the two lines, $\frac{F_{in}(H\alpha)}{F_{in}(H\beta)}$, (which is in a range of 2.86-3.0 depending on the electron temperature of the line emitting gas, from high to low). Applying the observed and intrinsic fluxes of H α and H β to equation

$F_{in}(\lambda) = F_{ob}(\lambda)e^{\tau(\lambda)}$ and combining with the above extinction curve, we get

$$\tau_V = - \frac{\ln \left[\frac{F_{ob}(H\alpha)}{F_{ob}(H\beta)} \right] - \ln \left[\frac{F_{in}(H\alpha)}{F_{in}(H\beta)} \right]}{\left[\left(\frac{\lambda_{H\alpha}}{5500} \right)^{-0.7} - \left(\frac{\lambda_{H\beta}}{5500} \right)^{-0.7} \right]} \quad (2-4)$$

Therefore, $\tau(\lambda)$ can be calculated for any wavelength, so the intrinsic flux and the luminosity from a star can be calculated through $F_{in}(\lambda) = F_{ob}(\lambda)e^{\tau(\lambda)}$ and $L_{in}(\lambda) = 4\pi D^2 F_{in}(\lambda)$, where D is the distance.

In SDSS J1500+4528, since there are two line components, we calculated τ_V using combinations of different $\frac{F_{ob}(H\alpha)}{F_{ob}(H\beta)}$ and two different theoretical ratio values, $\frac{F_{in}(H\alpha)}{F_{in}(H\beta)}$. The resultant six τ_V values are recorded in Table 2-3, where H α blue and H β blue mean the blue-shifted components. The largest extinction is for the emission line component centered at the rest wavelength (Balmer decrement 4.77). We take $\tau_V=2.47$ (corresponding to the theoretical value of 2.86) as an upper limit of the extinction in this galaxy. We also consider the Balmer decrement derived from the total (blue-shifted + unshifted) line fluxes as a reasonable value, and take the smaller value $\tau_V=1.76$ as a lower limit of the extinction in this galaxy.

After calculating the extinction value, the intrinsic flux and luminosity can be calculated using the equations above, for various τ_V values listed in Table 2-3. We list in Table 2-1 the highest and lowest possible intrinsic luminosities calculated by using the upper and lower limits of τ_V .

Table 2-3 The value of τ_V for different parameters in SDSS J1500+4428

| Observed ratio / Theoretical ratio | $\frac{F_{ob}(H\alpha)}{F_{ob}(H\beta)} = 4.77$ | $\frac{F_{ob}(H\alpha\text{blue})}{F_{ob}(H\beta\text{blue})} = 3.93$ | $\frac{F_{ob}(H\alpha+H\alpha\text{blue})}{F_{ob}(H\beta+H\beta\text{blue})} = 4.32$ |
|------------------------------------|---|---|--|
| 2.86 | 2.47 | 1.53 | 1.99 |
| 3.0 | 2.24 | 1.30 | 1.76 |

For NGC4395, there is only component of the H α and H β line, τ_V is estimated using different

theoretical ratios. Accordingly, τ_v equals 2.88 and 2.65 when the theoretical ratio 2.86 and 3.0 is used, respectively. In this work we assume the extinction value to be $\tau_v=2.65$ and calculate the intrinsic luminosities of the emission lines (given in Table 2-2).

2.3.3. Estimating the metal abundance of the ionized gas region

Studies showed that the process of star formation and the resultant initial mass function are dependent on the amount of metals (elements heavier than helium) existing in the gas. We use oxygen-to-hydrogen ratio to represent metal abundance, assuming that the relative abundances of various metal elements are the same as the solar abundances. To measure the oxygen abundance, we adopt the method of Pettini & Pagel (2004). The metal abundance can be measured from the ratio of the luminosity of NII line (6583Å) to H α line (6563Å), as shown in formula below.

$$12 + \log(O/H) = 0.57 \log[I([NII])/I(H\alpha)] + 8.90 \quad (2-5)$$

For SDSS J1500+4528, the oxygen abundance is obtained $12 + \log(O/H) = 8.80$. Taking the solar oxygen abundance $[12 + \log(O/H)]_{\odot} = 8.93$, we derive the metal abundance to be $Z = 0.77Z_{\odot} = 0.0154$, where Z_{\odot} represents the solar metal abundance ($Z_{\odot} = 0.02$). For NGC4395, we estimate the oxygen abundance $12 + \log(O/H) = 8.2$. Then the metal abundance is $Z = 0.16Z_{\odot} = 0.0033$.

Based on our estimation, the metal abundance of SDSS J1500+4528 is similar to the solar value, whereas NGC4395 has a low metal abundance.

2.3.4. Estimating the electron density of the line-emitting gas

The relative strengths of some emission lines are related to the electron density of the line emitting gas (but insensitive to other parameters such as temperature). They thus can be used to determine the electron density. One commonly used line pair is the doublet SII6717 and SII6731. We estimate the electron density using the line ratio vs. density curve presented in the figure in Osterbrock (1989). From the line ratios in the above Table and assuming a gas temperature of 10,000 K, which is typical for line-emitting gas in ionization-recombination equilibrium, we get $n_e \approx 300 \text{ cm}^{-3}$ for SDSS J1500+4528 and $n_e \approx 50 \text{ cm}^{-3}$ for NGC 4395. These values will be used in the estimation of the mass of the line-emitting regions in below.

3. The number of massive stars

3.1. Estimation of the number of W-R stars

The number of W-R stars is estimated using the luminosity of the blue and red bump. First, we estimated the number of WC stars using the luminosity of the red bump, CIV $\lambda 5808$. The following formula is used, where $L_{WC}(\lambda 5808)$ is the luminosity of the red bump, and L_{WC}^0 is the luminosity of one WC star (Schaerer D. & Vacca 1998).

$$N_{WC} = \frac{L_{WC}(\lambda 5808)}{L_{WC}^0} \quad (3-1)$$

The ratio of WC stars' contribution to the blue and red bump is described in formula below.

$$k = \frac{L_{WC}(\lambda_{4658})}{L_{WC}(\lambda_{5808})} \quad (3-2)$$

Using this formula, we can calculate WC stars' contribution to the luminosity of the blue bump. The blue bump comes from only WC and WN stars, so contribution of the WN stars can be calculated using formula, where L_{bb} represents total luminosity of the blue bump.

$$L_{WN} = L_{bb} - k \times L_{WC}(\lambda_{5808}) \quad (3-3)$$

Then, the number of WN stars can be calculated using above formula, where L_{WN} is the luminosity of WN's contribution to the blue bump, and L_{WN}^0 is the luminosity of one WN star.

$$N_{WN} = \frac{L_{WN}}{L_{WN}^0} \quad (3-4)$$

For L_{WN}^0 , the luminosity of a single WN star, we use $L_{WN}^0 = 2.0 \times 10^{36} \text{ erg/s}$ when $Z < Z_{\odot}$, and $L_{WN}^0 = 2.6 \times 10^{36} \text{ erg/s}$ when $Z > Z_{\odot}$ (Schaerer D. & Vacca 1998).

3.2. Estimation of the number of O stars

The number of O stars can be calculated using the H_{β} line (Guseva et al. 2000). The number of ionized photons is related to the luminosity of H_{β} line, as shown in formula below.

$$L(H_{\beta}) = 4.76 \times 10^{-13} Q_0 \quad (3-5)$$

W-R stars and O stars both contribute to the amount of ionizing photons. We adopt the amount of photons of W-R and O stars to be $Q_0^{WR} = Q_0^{O7V} = 1.0 \times 10^{49} \text{ s}^{-1}$. Here we use O7V to calculate the "number of O stars" if all O stars are O7V, then we can use the number combined with parameter η_0 to calculate the actual number of O stars. η_0 is the ratio of the number of O7V stars to the number of all O stars. The number of O stars is calculated using formula below.

$$N(O) = \frac{Q_0 - N_{WR} Q_0^{WR}}{\eta_0 Q_0^{O7V}} \quad (3-6)$$

3.3. Number of massive stars

3.3.1. Number of massive stars in SDSS J1500+4528

For SDSS J1500+4528, the red bump is not detected, so there is no WC star. The luminosity of the blue bump comes only from WN stars. It equals the sum of the NIII (4640Å), CIV (4650Å) and HeII (4686Å) luminosities. Based on the analysis above, there is a range of possible extinction values, ranging from $\tau_v = 1.76$ to $\tau_v = 2.47$. Since there is an uncertainty range for the actual internal extinction, we use the largest and the smallest τ_v to calculate the intrinsic blue bump luminosity in order to give the range. The intrinsic blue bump luminosity $L_{bb} = 3.43 \times 10^{42} \text{ erg/s}$ for $\tau_v = 1.76$ and $7.61 \times 10^{42} \text{ erg/s}$ for $\tau_v = 2.47$. Then the number of WN stars calculated is in the range from 1.7×10^6 to 3.8×10^6 , depending on the actual extinction value.

The total number of W-R stars and O stars (represented as W-R + O stars) is estimated using H_{β} luminosity, which ranges from 5.79×10^{42} to 1.26×10^{43} , corresponding to the minimum and maximum τ_v values. The number of W-R + O stars is 1.2×10^6 and 2.6×10^6 accordingly, which are both smaller than the number of W-R stars, though they are of the same order of

magnitude. This means that there might be no O stars considering the large uncertainty in the estimation. However, the real situation may be more complicated.

The line luminosities and estimated number of massive stars are listed in Table 3-1 line luminosities and the estimated number of massive stars

3.3.2. *Number of massive stars in NGC4395*

For NGC 4395, the red bump is obviously detected, centered at 5808Å. Civ λ 5808 is a strong emission line contributed by WC stars, and hardly comes from in WN stars. The CIII (5696Å) line is not found, indicating that the WC stars should be early types, likely WC4. The luminosity of the red bump is 5.5×10^{37} erg/s, thus the number of WC stars is estimated to be 18.

The total blue bump luminosity is greater than the contribution of WC stars, meaning that there are also WN stars. According to formula 3-3, $L_{WN} = 5.7 \times 10^{37}$ erg/s. Thus, there are 29 WN stars. The total number of W-R stars is 47.

Since the luminosity is 2.1×10^{37} erg/s, the estimated number of W-R + O stars is only 4, which is less than the number of W-R stars by one order of magnitude. Clearly, the number of massive stars estimated from the H β line luminosity is much smaller than and in contradictory to that of W-R stars from the W-R features. The number of W-R stars estimated using W-R feature is direct and thus reliable. However, the H β line luminosity depends not only on the number of massive stars but also on the conditions of the HII region. Thus, the number of massive stars estimated using this method is questionable. This problem will be discussed in section 2.3.

Table 3-1 summarizes the line luminosities and the estimated number of massive stars for both galaxies.

Table 3-1 line luminosities and the estimated number of massive stars

| | SDSS J1500+4528 | | NGC 4395 |
|---|---------------------|---------------------|----------|
| | ($\tau_v = 1.76$) | ($\tau_v = 2.47$) | |
| Blue bump luminosity (10^{38} erg/s) | 3.43×10^4 | 7.61×10^4 | 1.5 |
| red bump luminosity (10^{37} erg/s) | - | - | 5.5 |
| H β luminosity(10^{37} erg/s) | 5.79×10^5 | 1.26×10^6 | 2.1 |
| Number of ionizing photons ($10^{49}s^{-1}$) | 1.2×10^6 | 2.6×10^6 | 4.5 |
| Number of W-R stars | 1.7×10^6 | 3.8×10^6 | 47 |
| W-R + O stars from ionizing photons | 1.2×10^6 | 2.6×10^6 | 4 |

4. Results and physical interpretation

4.1. Summary of results

4.1.1. SDSS J1500+4528

- 1) A candidate Wolf-Rayet galaxy with a possible large number of Wolf-Rayet stars, SDSS J1500, was selected from the SDSS data archive.
- 2) The spectral analysis is carried out, and the emission line parameters are measured. The results confirm that SDSS J1500+4528 is indeed a W-R galaxy, hosting W-R stars that are descendants of the most massive stars ($M > 25-35 M_{\odot}$) that can possibly form.
- 3) Strong extinction in the star-forming region is found.
- 4) We counted the number of W-R stars to be $N=3.8 \times 10^6$ using the luminosity of the W-R blue emission bump (or a factor of ~ 2 less for a smaller extinction value in the galaxy). This number is more than what is needed to produce the H β luminosity observed, suggesting apparently there may be no O star, or at least of not in large number.
- 5) We derived the metallicity for this galaxy to be 0.77 solar value from the NII/ H_{α} line flux ratio, and an electron density of $n_e \approx 300 \text{ cm}^{-3}$ from the doublet line ratio of SII.
- 6) We derived the age of the newly formed stellar population to be 5 Myr using the equivalent-width of the H β line and the result of massive star evolutionary model of Schaerer & Vacca (1998).
- 7) All the strong emission lines from the ionized gas region (except for the W-R emission features) have two gaussian components. One centers at the rest frame wavelength, with a typical linewidth of ~ 300 km/s. The other component is a bulk blueshift component. This broad component has a systematic blueshift velocity of 190 km/s and a width of 900 km/s (full width at half maximum). The lower velocity wing of this component extends to the red shift range. This result shows that we see the line emitting gas moving both towards and away from us. The gas moving towards us has greater amount and larger overall speeds, since

the blue-shifted portion is larger than the redshifted portion. These mean that the majority gas of this component is moving towards the observer and has greater velocity.

4.1.2. NGC4395

- 1) NGC4395 is a nearby galaxy which is also selected as a candidate of W-R galaxies, in order to compare with SDSS J1500 which is far away. We found the features of W-R stars in one of its star-forming regions, so it is certain that NGC4395 is a W-R galaxy. The number of W-R stars is estimated to be 47, including 29 WN stars and 18 WC stars.
- 2) However, we found a problem that the luminosity of H_{β} line is one order of magnitude lower than it is predicted for regions around massive stars.
- 3) Strong extinction in the star-forming region is found.
- 4) We derived the metallicity of 0.16 solar value from the NII/H_{α} line flux ratio, and an electron density of $n_e \approx 50 \text{ cm}^{-3}$ from the doublet line ratio of SII.

4.2. The greatest population of massive stars and extreme starburst

One of the most remarkable result in our study is the number of W-R stars found in SDSS J1500+4528, 3.8×10^6 (or 1.7×10^6 if the smallest possible extinction value is used). To our knowledge, this is the largest number of W-R stars ever found in a single galaxy. In previous studies, the number of W-R stars found in a single galaxy ranges from tens in normal galaxies up to $\sim 10^5$ in galaxies with ongoing star-formation. The W-R stars seen in SDSS J1500+4528 outnumbers these known W-R galaxies by about one order of magnitude or more.

The age of the star population we see can be determined. O stars have short lives of $3 - 5 \times 10^6$ years, and W-R stars take place at the last one tenth of O star's life, about 5×10^5 years. The W-R stars' progenitor O stars are formed 5 Myr ago, which mostly transformed into W-R stars by now. Thus, these W-R stars must be newly formed. In the above analysis, we estimated the age of the using the equivalent width of H_{β} line and stellar evolution model. It also turns out to be 5 Myr, which means that the W-R stars we see are formed in one star-formation episode as the rest of the stars in this galaxy. Thus, the star-formation phase lasts at most 5 Myr. According to the initial mass function of star-formation, W-R stars are only the tip of iceberg of the entire star population in one star-formation event, so there must be a much greater number of stars formed. In fact, the total mass of newly formed stars can be estimated to be $5 \times 10^9 M_{\odot}$ by fitting the stellar spectrum using a stellar synthesis model (see Figure 7 in Schaerer D. & Vacca 1998) The average star formation rate is then at least $10^3 M_{\odot}/yr$. Thus, we conclude this galaxy experienced an intensive starburst.

4.3. Galactic fountain in SDSS J1500+4528

4.3.1. The galactic outflow and fountain

We see two regions of line emitting gas. One is at rest relative to the galaxy and the star forming region. Its linewidth represents Doppler broadening with a velocity dispersion of ~ 300

km/s, which is consistent with the random motion velocity dispersion of gas in galaxy. To our surprise, there is also a bulk blue shift component. The blueshift indicates an outflow of the line emitting gas which is moving towards the observer, that is to say, moving away from the galaxy. It means gases are lifted up from the galactic disk. The bulk of the gas (represented by the peak of the emission line) has a systematic blueshift velocity of 190 km/s as projected along our line of sight $v(\cos\theta) = 190$ km/s, where θ is the (unknown) angle between the line of sight and the direction of outflow velocity. The line is very broad, with a linewidth of 900 km/s (full width at half maximum), which means that the gases have a wide velocity range. The largest projected velocity can be as high as ~ 1000 km/s. The lower velocity wing extends to beyond velocity zero and to the redshift range as high as -570 km/s. These gases with velocity in the opposite direction represents an inflow of gas moving towards the galaxy, or falling back to the galactic disk. These gases have smaller amount of mass and lower speed compared to that of the outflow. We interpret them to be the part of the outflow that have velocity lower than the escape velocity and thus are pulled back by gravity. This phenomenon involving both outflow and inflow gases is known as the galactic fountain.

Outflows are often detected in starburst galaxies. These outflows are bi-polar, blowing gases away from both sides of the plane. The best-studied example is the bi-polar outflows in the nearby starburst galaxy M82 (Figure 4-1) which is viewed edge-on. Typical outflows can have a size as large as 10 lightyears in radius, and can reach a height of several tens of thousand lightyears above the galactic disk. Observations show that there are outflows of cold, warm, and hot gases in the same galaxy. Gases that radiate $H\beta$ lines are warm, at typical temperature of $\sim 10^4$ K (Osterbrock 1989). The warm gas emitting optical emission lines have typical outflow velocity of several hundred km/s (~ 600 km/s for M82) (Heckman & Thompson 2019). Therefore, the velocity of outflow gases found in SDSS J1500+4528 is consistent with those of the optical line emission gas in known starburst galaxies, suggesting that they are of the same phenomenon.



Figure 4-1 Example of outflowing gas in the famous nearby starburst galaxy M82 (optical light in white-blue color and the hydrogen emission line $H\alpha$ in red). Two large-scale bi-polar outflows (red colored), which are traced by the hydrogen emission lines, are seen perpendicular to the galactic disk. Note that both the bi-polar outflows are seen because the galaxy is viewed from the side of its disk.

If we are looking at the galaxy from its side, we can see both outflows on each side of the galactic disk, just like the figure of M82. In this case, we should detect two almost the same lines without systematical blue- or redshifts. If we look at a slightly tilted angle, we still can see two

symmetrical emission lines on both side of the rest wavelength, one blue-shifted and one redshifted, with similar maximum velocities. Since we only observed one emission line in SDSS J1500+4528, we are likely seeing only one side of the outflow and the other is obscured by the galactic disk. This means that we see the galaxy at an angle close to face-on or at a moderate inclination angle to the galactic disk plane.

This is the first time that an outflow is discovered in Wolf-Rayet galaxies, and the first time seeing a very likely fountain-like one, to our knowledge.

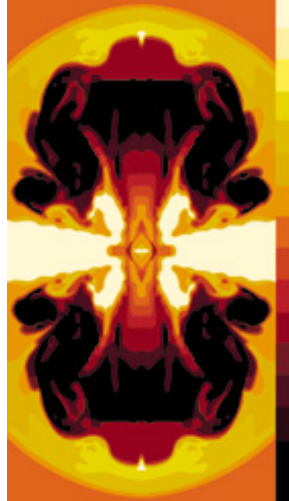


Figure 4-2 Computer simulation of bi-polar galactic fountains formed in a star-forming galaxy. An outflow is launched driven by supernova explosion. The outer part with low speeds turns downwards and fall back. (Figure from Internet)

4.3.2. The driving energy of the outflow

It is widely accepted that strong outflows in stars forming galaxies are driven by explosion energy of supernovae which are the end of the life of massive stars. We examine this possibility by estimating the energy required to drive the wind.

We need to estimate the mass of outflowing gas first. The total mass of H_{β} emission region is estimated from the luminosity $L(H_{\beta})$, or the number of ionizing photons that leave the star per unit time, Q . In the condition of ionization equilibrium, the recombination rate equals the ionization rate Q . Based on equations 5.21 and 5.22 in the textbook by Maoz (2007), we have

$$Q = \mathcal{R}_{re}V = \alpha(T)n_en_pV = \alpha(T)n_eN_p$$

where $\mathcal{R}_{re} = \alpha(T)n_en_p$ is the number of recombination of electrons and protons per unit time per unit volume, $\alpha(T)$ is the recombination coefficient, n_e and n_p are the number density of electrons and protons, V is the volume of H_{β} emission region, and N_p the total number of protons. Thus,

$$N_p = \frac{Q}{\alpha(T)n_e}$$

The mass of hydrogen is $M_p = m_p N_p$, where m_p is the effective mass of a proton $1.67 \times 10^{-24} g$ (the mass of a pair of proton and electron). Assuming a solar abundance in the region, that is, the mass fraction of hydrogen is 75%, the total mass can be estimated by

$$M = \frac{M_p}{0.75} = \frac{m_p N_p}{0.75} = \frac{1.67 \times 10^{-24} Q}{0.75 \alpha(T) n_e}$$

We take $\alpha(T) = 2.6 \times 10^{-13} cm^3 s^{-1}$ at $T \sim 10^4 K$ from Maoz (2007). The electron density, $300 cm^{-3}$, is estimated from the SII line ratio in section 2. The number of ionizing photons per second, $Q = 2.6 \times 10^{55} s^{-1}$, has been calculated from the H β luminosity of the blueshift component (Table 2-1) using equation (3-5). Note that here we use the upper end value of the possible range because we want to examine the case of the highest energy needed. The electron density $n_e = 300 cm^{-3}$ is determined from the SII doublet line ratio as above. Thus, the mass of the outflow is calculated using

$$M = 7.42 \times 10^{41} g = 3.73 \times 10^8 M_\odot \text{ for SDSS J1500+4528}$$

Taking the average velocity of the gas to be $190 km s^{-1}$, the total kinetic energy of the outflows is

$$E_K = \frac{1}{2} M v^2 = 1.20 \times 10^{56} \text{ ergs}$$

This amount of energy is so large that only supernova explosion can provide, as widely believed. A single supernova's kinetic energy is $10^{51} erg$, and about $\eta = 10\%$ is then transferred to the kinetic energy of gas. It therefore requires

$$N_{SN} = \frac{E_k}{\eta 10^{51}} \approx 1.2 \times 10^6$$

supernovae to drive the outflow. This number of supernovae, i.e. O stars that have died, is comparable to that of the W-R stars. This means that a significant fraction of O stars has died and the rest evolved into W-R stars that we observed. Thus, the number of W-R stars and the observed outflow gas are physically consistent.

Our result is consistent with the supernovae driving scenario. The star-formation happened 5 Myr ago appears to have been weakened or even stopped now. This can be explained by that the strong outflow blows away the gas and molecular clouds in the star forming region. This effect is called feedback.

A fraction of the gas has velocities larger than the escape velocity (several hundred km/s). They can reach as far as more than ten thousand light years away from the galaxy. In this case, these emission lines produced by these gases cannot be collected by the fiber in the SDSS observation. This may explain the apparently lower H β luminosity compared to value expected from the number of massive stars. Some O stars might still exist.

4.4. Initial mass function of the star-formation.

Since we have calculated the number of massive stars, we can use this to constraint the initial mass function of star-formation. The Salpeter initial mass distribution (Salpeter 1955) is

$$dN = Cm^{-2.35} dm$$

The total mass of stars which have mass in the range of $0.4M_{\odot} < m < 20M_{\odot}$ can then be integrated,

$$M = \int_{0.4}^{20} mdN = \int_{0.4}^{20} Cm^{-1.35} dm = \frac{C}{0.35} (0.4^{-0.35} - 20^{-0.35}),$$

where M is in units of solar mass. With known mass M, we get

$$C = \frac{0.35M}{0.4^{-0.35} - 20^{-0.35}}$$

And the number of stars with mass larger than 25 solar mass, which are bound to evolve into W-R stars eventually, is

$$\begin{aligned} N &= \int_{25}^{150} dN = \int_{25}^{150} Cm^{-2.35} dm = \frac{C}{1.35} (25^{-1.35} - 150^{-1.35}) \\ &= \frac{0.35M}{0.4^{-0.35} - 20^{-0.35}} \frac{25^{-1.35} - 150^{-1.35}}{1.35} \end{aligned}$$

For independently determined total mass of newly formed stellar population $M = 5 \times 10^9 M_{\odot}$ for SDSS J1500, the number of stars that are bound to evolve to W-R stars is theoretically predicted to be 1.5×10^7 . This number is 5 times the number of W-R stars we derived from observational data, implying: i) there are actually 5 times the number of massive stars we find, and most of them might have evolved and exploded as supernovae; ii) the initial mass function (IMF) for the massive stars are steeper than low mass stars; or iii) the whole power law of IMF is steeper than that given by Salpeter (1955).

In the case of i), the number of supernovae is much larger than the number required to drive the outflow we observe. Thus, we consider it unlikely.

In the case of ii), the IMF index at the high mass end ($m > 20M_{\odot}$) can be derived from the observed number of W-R stars by assuming a different power law slope,

$$dN_h = C_h m^{-\alpha} dm$$

The normalization parameter C_h is determined from the smooth connection of the IMF at $m = 20M_{\odot}$, i.e. from $C_h m^{-\alpha} = Cm^{-2.35}$,

$$C_h = 20^{-2.35+\alpha} C = 20^{-2.35+\alpha} \frac{0.35M}{0.4^{-0.35} - 20^{-0.35}}$$

Therefore, the number of massive stars with $m > 25M_{\odot}$ can be expressed as

$$N = \int_{25}^{150} dN = 20^{-2.35+\alpha} \frac{0.35M}{0.4^{-0.35} - 20^{-0.35}} \frac{25^{-\alpha+1} - 150^{-\alpha+1}}{\alpha - 1}$$

Now we compare the predicted number of massive stars N with the observed number of W-R stars, $N_{W-R} = 3 \times 10^6$. Assuming $N = 2N_{W-R}$, then the number of initial massive stars is around 6×10^6 . Some of the massive stars have already evolved and exploded as supernovae, and some might have missed from the O star number estimation from the $H\beta$ line due to the reason discussed below. In this case, from the above equation, the IMF index $\alpha=3.7$. This value is

significantly larger than that of Salpeter (1955). If more stars have evolved into supernovae, say, twice of the number of W-R stars, $N = 3N_{W-R} = 9 \times 10^6$. Then, the index $\alpha=3.0$. Based on the number of required supernovae, we consider this case is reasonable. Thus, a greater index than the Salpeter value at the massive end of the IMF is possible. Such a value has also been claimed in other studies (e.g. $\alpha=3.3$, see Zhang 2007).

For case iii), adopting a power law of IMF, $dN = Cm^{-\alpha}dm$, the coefficient C is a function of index α , so is the number of massive stars,

$$C = \frac{(\alpha-2)M}{0.4^{-\alpha+2}-20^{-\alpha+2}},$$

$$N = \int_{25}^{150} dN = \int_{25}^{150} Cm^{-\alpha}dm = \frac{(\alpha-2)M}{0.4^{-\alpha+2}-20^{-\alpha+2}} \frac{25^{-\alpha+1}-150^{-\alpha+1}}{\alpha-1}$$

Given the mass M in range of $0.4M_{\odot} < m < 20M_{\odot}$ and the number N of massive stars evolved into W-R star and supernovae, $N = 6 \times 10^6$, $M = 5 \times 10^9 M_{\odot}$, we derive $\alpha=2.6$ from the above equation, which is slightly larger than 2.35 given by Salpeter. If the number of massive stars evolved into supernovae is 2 times of that evolved into W-R stars, the index can be slightly smaller $\alpha=2.5$.

In conclusion, a greater index (steeper power law) at the massive end of the IMF, or a steeper overall IMF slope is preferred. Given the relatively high metallicity of this galaxy, $Z = 0.77Z_{\odot}$, this conclusion is consistent with previous studies that the IMF becomes steeper at higher metallicities (Zhang et al, 2007).

4.5. NGC4395: a local galaxy with star-forming regions

NGC4395 is a nearby galaxy with many star-formation regions. We include the data of this galaxy as a comparison study. We found about 47 W-R stars (including 29 WN stars and 18 WC stars) in one of the star-formation regions covered by one of the fibers in the SDSS observation. This number is typical of massive stars in on-going star-formation regions in nearby galaxies. This confirms the results of our estimation of W-R star number, justifying that our results for the distant galaxy SDSS J1500+4528 is reliable. No outflow gas component is found, from the hydrogen emission line profiles.

We notice in our result that the luminosity of H β line is one order of magnitude lower than it is predicted for an ionized gas region around W-R stars, even considering the ionization from the observed W-R stars only (and ignoring possible O stars). The most likely explanation is that, similar to the case of SDSS J1500+4528, a substantial amount of the gas close to the W-R stars (and also possible O stars) stars has been blown away to far distance by the strong radiation pressure and outflows from these stars. Since the galaxy is relatively close-by, the SDSS fiber covers only a region of 3 arcseconds or 215 lightyears in diameter (Figure 4-3; one second of arc corresponds to 71.8 lightyears at this distance). Within this region the gas might have been largely evacuated. As a result, the entire line-emitting gas region ionized by the massive stars must be extending beyond the area covered by the SDSS observing fiber. This leads to a large fraction of the emission line photons failed to be collected in the SDSS observation, as what is found in our result. The same effect may also affect the H β luminosity in SDSS J1500+4528, though to a

smaller extent.

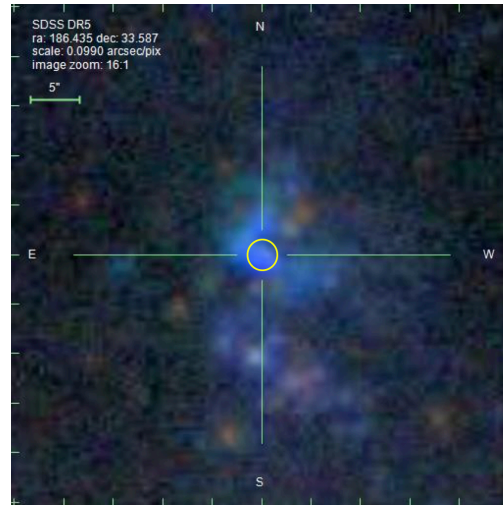


Figure 4-3 The optical image of the star-forming region in the galaxy NGC 4395 that was observed in the SDSS survey. The circle represents the region covered by the observing fiber, with a diameter of 215 lightyears. The light within this area was collected to produce the observed optical spectrum (image provided from the SDSS).

2020 S.-T. Yau High School Science Award

5. Summary

The most massive stars, which are very rare, play a critical role in helping us determine the mechanism and properties of star-formation. In this study, we focus on the most massive stars in the universe, Wolf-Rayet (W-R) star, which is the last stage of evolution of O stars before dying. We study two candidates of galaxy having W-R stars (W-R galaxies), SDSS J1500+4528 and NGC4395, using their optical spectral data taken in the Sloan Digital Sky Survey. Our aim is to search for and study galaxies with as many W-R stars as possible. SDSS J1500+4528 is such a candidate (provided by one of the supervisors). NGC 4395 is included in the study as a comparison for it is a nearby galaxy. Through analyzing their optical spectral data and measuring the emission lines, we find emission features of W-R stars, confirming they are indeed W-R galaxies. The number of W-R stars can be easily counted using the integrated luminosities of their emission features, based on the previously determined luminosity for a single W-R star.

The number of W-R stars in SDSS J1500+4528 is estimated to be about three million, which outnumbers those found in previous studies. The number can be used to constrain the slope of the initial mass function, which is the rate of star-formation at various masses. The age of the newly formed stellar population is inferred to be 5 million years, so most of the massive stars are just at the end of their lifetimes. There appears no need for the presence of a large number of other massive stars (O stars) based on the observed $H\beta$ emission line luminosity, which can be understood as O stars having already died away and/or the line-emitting gas region being too extended to be observed.

To our surprise, all strong emission lines from the ionized gas region (not from the W-R stars) have two gaussian components. One centers at the rest frame wavelength, associated with the newly formed stellar population. The other broad component shows a bulk Doppler blueshift relative to the former, corresponding to a systematic velocity of 190 km/s projected toward the observer. This component is strongly Doppler broadened by a wide range of velocities, and actually its lower velocity wing extends to the red shift range. This result paints a fascinating picture of dynamic line-emitting gas clouds moving, at velocities spanning a wide and continuous range, both away from and towards the galactic disk. This phenomenon is called the galactic fountain, which is seen in W-R galaxies for the first time. The kinetic energy of the gases blown away from the galactic disk is calculated to be a tremendous amount. This energy can be accounted for as being driven by supernovae explosions, with their number comparable to that of the W-R stars, as the spectacular ending of the lives of massive stars.

Even though the number of massive stars (WR-stars plus possible progenitors of supernovae) inferred in this galaxy is huge, it is still much less than the theoretical number predicted from the initial mass function (IMF) assuming the commonly accepted value of the IMF index. We also discussed the constraint of our results to the IMF at the high-mass end.

The number of W-R stars in one of the star-forming regions of NGC4395 is estimated to be 47, including 29 WN stars and 18 WC stars. However, the luminosity of $H\beta$ line is one order of magnitude lower than it should be for a line-emitting ionized gas region around W-R stars. We explain this as that a large amount of the gases around W-R stars has been blown away by the strong radiation and outflows of the W-R stars, so that the line-emitting region is

much extended beyond that can be covered by the observation.

To summarize, we discovered the so far greatest number of massive stars in the Wolf-Rayet phase in a galaxy experiencing recent immense star-formation. To our surprise a strong gas outflow, in the form of a galactic fountain, is also discovered in this galaxy, for the first time in Wolf-Rayet galaxies. We show that the fountain can be explained as being driven by the explosions of supernovae when the massive stars come to the end of their lives.

2020 S.-T. Yau High School Science Award

References

- Agienko K.B., et al. Sample of wolf-rayet galaxies from the sloan digital sky survey, *Kinematics and Physics of Celestial Bodies*, 2013, Vol. 29, No. 3, pp. 131–140. © Allerton Press, Inc. ISSN 0884-5913
- Allen D.A., et al., The dwarf emission galaxy hea-io, 1976 *MNRAS*, 177, 91
- Charlot S. & Fall S.M. A simple model for the absorption of starlight by dust in galaxies, 2000, *ApJ* 539, 718
- Conti P. Wolf-rayet galaxies: an introduction and a catalog, 1991, *ApJ*, 377, 115
- Fitzpatrick E.L., Correcting for the Effects of Interstellar Extinction, *Publications of the Astronomical Society of the Pacific* 1999, 111, 63
- Heckman T.M. & Thompson T.A., A brief review of galactic winds, arXiv:1701.0906v2, 2019
- Liang F.-H., et al. Wolf-Rayet galaxies in SDSS-IV MaNGA. I. Catalog construction and sample properties, 2020 *ApJ*, 896, 121
- Maoz D. *Astrophysics in a nutshell* 2007, Princeton Universtiy Press
- Osterbrock D. E. & Cohen R. D. Two galaxies with wolf-rayet features in their spectra, 1982 *ApJ*, 261, 64
- Osterbrock D.E., *Astrophysics of Gaseous Nebulae and Active Galactic Nuclei* (University Science Books: Mill Valley) 1989
- Pettini M. & Pagel B.E. J. [O III]/[N II] as an abundance indicator at high redshift, 2004 *MNRAS*, 348, L59
- Salpeter E.E., The Luminosity Function and Stellar Evolution, 1955, *ApJ* 121, 161
- Schaerer D. & Vacca W.D., New models for wolf-rayet and o star populations in young starbursts, 1998, *ApJ* 497, 618
- Vacca W. & Conti P.S., Optical spectrophotometry of Wolf-Rayet galaxies, 1992 *ApJ*, 401, 543
- Zhang W., et al. Wolf-rayet galaxies in the sloan digital sky survey: the metallicity dependence of the initial mass function, 2007 *ApJ*, 655, 851
- 张伟 基于斯隆数字巡天的大样本沃尔夫-拉叶星系研究 Wolf-rayet galaxies in the sloan digital sky survey (中国科学技术大学 博士学位论文) 2007

Acknowledgement/致谢

首先感谢两位导师周宏岩教授和仲国虎博士的精心指导。两位老师从开题报告到论文撰写及修改都给予了很好的建议和悉心的指导，周老师还从百忙中对项目的相关背景知识进行了一对一讲解。其次，感谢本校负责丘赛的范博昭老师的全程教导和督促，范老师的博学 and 严谨是我顺利完成项目的必不可少的。在使用 SDSS 数据过程中还得到过国家天文台刘禾阳博士的指导，在此一并致谢。

2020 S.-T. Yau High School Science Award